the energy transfer mechanisms differ, particularly with respect to the transfer of baseflow energy to fluctuations. It is significant to observe in the Couette viscometer case that although a transition does occur at a certain critical angular speed, the resultant flow is not turbulent but rather a stabilized secondary cellular motion. Therefore, although Equation (6) clearly indicates instability for the cylindrical Couette case for all rotational speeds, the different energy transfer mechanism caused by the moving boundary apparently stabilizes the flow into at least two nonturbulent modes, the distinction between which requires a different type of analysis (5) to make.

As a result of the above observations it appears that the present theory accurately predicts profile instability and transition to turbulent motion in stationary boundary flows but predicts only velocity profile instability in moving boundary flows. Since the present theory deals only with profile stability, no quantitative predictions can be made concerning the energy transfer mechanism and other theories (5) must be relied upon in moving boundary cases to predict transitions between the stabilized nonturbulent motions.

Graphical Calculation of Multiple Steady States and Effectiveness Factors for Porous Catalysts

WARREN E. STEWART

University of Wisconsin, Madison, Wisconsin

and

JOHN V. VILLADSEN

Instituttet for Kemiteknik, Danmarks tekniske Højskole, Copenhagen, Denmark

Simple graphical methods are given for predicting the effectiveness factors of single reactions in particles of various shapes. A collocation procedure is used for small particles, and the known asymptotic solution is used for large particles. Multiple steady states and variable fluid properties can be handled directly. Examples are given for several nonlinear reaction rate laws.

The prediction of catalyst effectiveness factors for nonlinear situations is a continuing problem in process design and research. Such calculations can be done routinely by conventional finite-difference techniques, but this approach gives little insight, and permits dangerous misinterpretations if multiple solutions are present. Similar criticisms apply to the use of generalized coordinates to extrapolate effectiveness factor plots from one reaction rate law to another.

Simple calculation methods are presented here for two ranges of particle size. The solution for large particles was derived by Stewart (*12*) for isothermal systems, and extended by Peterson (*10, 11*) to nonisothermal systems. The solution for small particles is obtained from a collocation principle given by Villadsen and Stewart (*13*); it gives detailed information about the number and location of the steady states. From these two asymptotic solutions, useful predictions can be made for all particle sizes.

STATEMENT OF THE PROBLEM

Consider a single chemical reaction at steady state in a porous particle, with n fluid species present. The mass and energy conservation equations are taken as:

$$(\nabla \cdot \mathcal{D}_i \nabla c_i) = -R_i \quad i = 1, \ldots n \tag{1}$$

$$(\nabla \cdot k \nabla T) = -\sum_{i=1}^{n} (\nabla \cdot \overline{H}_i \mathcal{D}_i \nabla c_i) \tag{2}$$

The production rates of the species per unit particle volume are expressed as

$$R_i = \nu_i R_A (c_1, \ldots c_n, T) \quad i = 1, \ldots n \tag{3}$$

in which A is a species chosen as a basis for calculations. This equation also defines ν_i, the stoichiometric coefficient for species i relative to A. The conditions on the outer boundary of the particle are considered to be constant:

$$\text{on } S_p, \begin{cases} c_i = c_{i0} & i = 1, \ldots n \quad (4) \\ T = T_0 & \quad (5) \end{cases}$$

Expressions for the profiles of temperature and concentration, and the effectiveness factor

$$\eta = \frac{1}{R_{A0} V_p} \iiint R_A \, dV_p, \tag{6}$$

are desired. Here R_{A0} is the production rate of species A at the outer surface conditions, and V_p is the volume of the particle. The quantities $\mathcal{D}_i$, k, $\overline{H}_i$ and R_A are considered to depend only on $c_1, \ldots c_n$ and T; that is, the particle is considered to be homogeneous and isotropic.

The quantities $\mathcal{D}_i$ and k are effective transport properties, defined by the abbreviated flux equations $\mathbf{N}_i = -\mathcal{D}_i \nabla c_i$ and $\mathbf{q}^{(c)} + \mathbf{q}^{(x)} = -k\nabla T$. All current theories of transport in porous media can be thus abbreviated, when use is made of the stoichiometric constraints $\mathbf{N}_i = \nu_i \mathbf{N}_A$ and $\mathbf{q}^{(c)} + \mathbf{q}^{(x)} = -\sum_{i=1}^{n} \overline{H}_i \nu_i \mathbf{N}_A$ that hold within the particle. These constraints are consistent with the steady state conservation equations for a homogeneous, isotropic particle under boundary conditions (4) and (5).

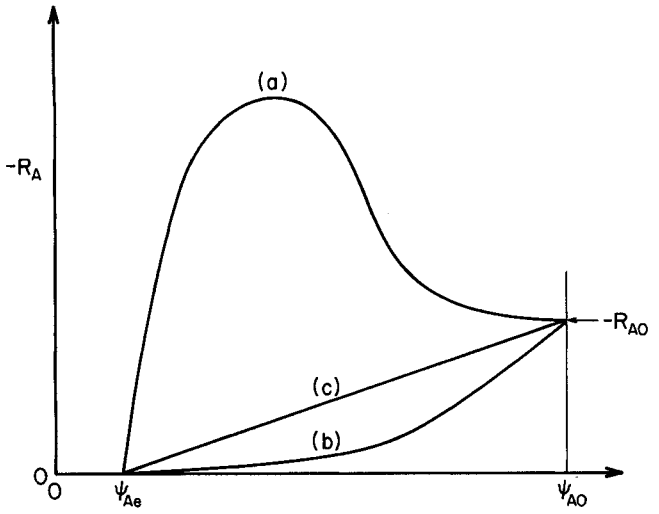

Fig. 1. Typical reaction rate curves based on a reactant species. (a) Exothermic reaction. (b) Endothermic reaction. (c) First-order isothermal reaction, constant diffusivities.

SIMPLIFICATION OF THE PROBLEM

Application of the stoichiometric constraints gives the differential relations

$$\frac{dc_i}{dc_A} = \nu_i \frac{\mathcal{D}_A}{\mathcal{D}_i} \quad i = 1, \ldots n \tag{7}$$

$$\frac{dT}{dc_A} = -\frac{\mathcal{D}_A}{k} \sum_{i=1}^{n} \nu_i \overline{H_i} \tag{8}$$

and eliminates all but one of Equations (1) and (2) from further consideration. If the right sides of Equations (7) and (8) are constant, then one obtains the wellknown relations

$$\mathcal{D}_i(c_i - c_{i0}) = \nu_i \mathcal{D}_A(c_A - c_{A0}) \quad i = 1, \ldots n \tag{9}$$

$$k(T - T_0) = \left(- \sum_{i=1}^{n} \nu_i \overline{H_i} \right) \mathcal{D}_A(c_A - c_{A0}) \tag{10}$$

Other forms of variation of the physical properties can be handled by integrating Equations (7) and (8) numerically. It is desirable to use the function

$$\psi_A = \int_{c_{A,\,\mathrm{ref.}}}^{c_A} \mathcal{D}_A dc_A \tag{11}$$

as the integration variable, to simplify this integration and the subsequent calculations. The reference state, with concentration $c_{A,\,\mathrm{ref.}}$, may be chosen according to convenience for the problem at hand.

The calculations just described permit R_A of Equation (3) to be plotted vs. ψ_A for a given set of external conditions (see Figure 1). The plot may be terminated at the equilibrium point ($R_A = 0$, $\psi_A = \psi_{Ae}$) since the reaction cannot go further. The problem then reduces to solving the differential equation

$$\nabla^2 \psi_A = -R_A(\psi_A) \tag{12}$$

with the boundary condition

$$\psi_A = \psi_{A0} \text{ on } S_p \tag{13}$$

Two procedures for this stage of the solution are given below.

SOLUTION FOR LARGE PARTICLES

With increasing particle size, and any given particle shape, the ψ_A profile approaches that for the same depth in an infinite catalyst slab. The local flux of species A through S_p is then given by

$$|N_{A0}| = \sqrt{2 \int_{c_{Ae}}^{c_{A0}} -R_A \mathcal{D}_A dc_A}$$

$$= \sqrt{2 \int_{\psi_{Ae}}^{\psi_{A0}} -R_A d\psi_A} \tag{14}$$

and the effectiveness factor is

$$\eta = \frac{S_p}{V_p |R_{A0}|} \sqrt{2 \int_{\psi_{Ae}}^{\psi_{A0}} -R_A d\psi_A} \tag{15}$$

for any rate function and any particle shape (*10, 11, 12*). The integral is just the area under the rate curve in the coordinates of Figure 1. These expressions give upper bounds on the true $|N_{A0}|$ and η for convex particles of any size.

SOLUTION FOR SMALL PARTICLES

For small particles, the profile ψ_A can be fitted well by a parabolic trial function, $\psi_A^{(1)}$, with one adjustable coefficient. The fitting is done here by the orthogonal collocation method of Villadsen and Stewart (*13*), which was developed for problems such as this. The following formulae are adapted from (*13*), where the principles of the method are given.

The trial functions, $\psi_A^{(1)}$, are given in Table 1. They correspond to the approximation $y^{(1)}$ of reference *13*. Each function has the form $a_0[1 - X^2] + \psi_{A0}$, where X is a coordinate that equals unity on S_p. Each function satisfies Equation (13) exactly for the given geometry, and satisfies Equation (12) in the limit of constant reaction rate (small particle size).

To fit these functions to a given reacting system, we adjust $a_0^{(1)}$ so that $\psi_A^{(1)}$ satisfies Equation (12) at a set of collocation positions within the particle. Following the technique of (*13*), we choose the positions as the zeroes of the second-degree polynomial $P(X)$ orthogonal to $\psi_A^{(1)} - \psi_{A0}$ over the particle volume. The positions are summarized in Table 1. These collocation positions give the best accuracy for the mean reaction rate, and also minimize the differential-equation residual, $\{\nabla^2 \psi_A^{(1)} + R_A[\psi_A^{(1)}]\}$, in a least squares sense.

Application of Equation (12) to the function $\psi_A^{(1)}$ at

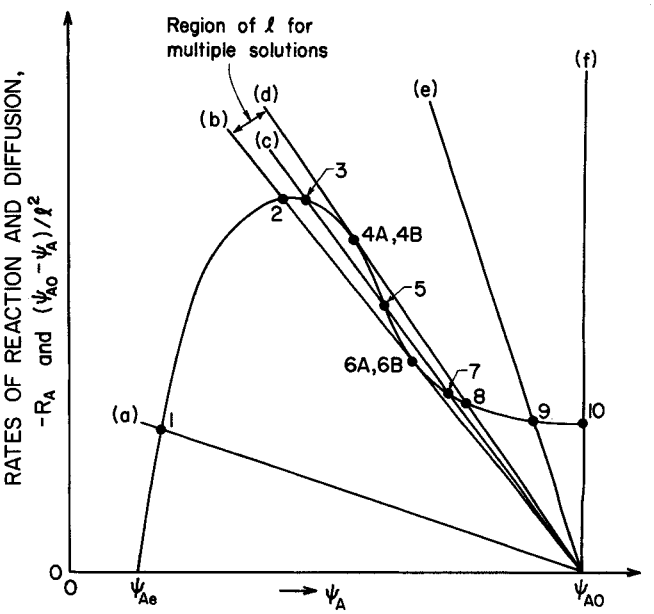

Fig. 2. Graphical solutions of Equation (16) for curve (a) of Figure 1. Points numbered twice are pairs of solutions. (a) Large particle; solution at 1. (b) Smaller particle; solutions at 2, 6A, 6B. (c) Smaller particle; solutions at 3, 5, 7. (d) Smaller particle; solutions at 4A, 4B, 8. (e) Smaller particle; solution at 9. (f) Zero particle size; solution at 10.

TABLE 1. FUNCTIONS AND CONSTANTS

Particle geometry	Trial function
infinite slab of thickness L	$\psi_A^{(1)} = a_0^{(1)} \left[1 - \left(\frac{2z}{L} \right)^2 \right] + \psi_{A0}$
long cylinder of diameter D	$\psi_A^{(1)} = a_0^{(1)} \left[1 - \left(\frac{2r}{D} \right)^2 \right] + \psi_{A0}$
sphere of diameter D	$\psi_A^{(1)} = a_0^{(1)} \left[1 - \left(\frac{2r}{D} \right)^2 \right] + \psi_{A0}$
ellipsoid with axes of lengths L_x, L_y and L_z	$\psi_A^{(1)} = a_0^{(1)} \left[1 - \left(\frac{2x}{L_x} \right)^2 - \left(\frac{2y}{L_y} \right)^2 - \left(\frac{2z}{L_z} \right)^2 \right] + \psi_{A0}$

the chosen positions gives the collocation equation

$$(\psi_{A0} - \psi_{A1})/l^2 = -R_{A1} \qquad (16)$$

for each geometry. Here ψ_{A1} is the value of $\psi_A^{(1)}$ at the collocation positions, and l is a characteristic length which depends on the particle size and shape (see Table 1). The term $(\psi_{A0} - \psi_{A1})/l^2 \equiv \nabla^2 \psi_A^{(1)}|_1$ is the rate of diffusion of species A into a unit volume element at the collocation positions, and the term $-R_{A1} \equiv -R_A(\psi_{A1})$ is the corresponding rate of consumption of A by the reaction.

Equation (16) can be solved graphically by plotting $(\psi_{A0} - \psi_A)/l^2$ and $-R_A$ vs. ψ_A, and noting the intersections (see Figure 2). For continuous rate functions that go to zero at equilibrium, there will be at least one solution for each particle size. Multiple solutions will occur if the diffusion line touches the reaction line more than once. The number of solutions is odd, in agreement with Gavalas (5), if tangencies are counted properly as multiple roots.

The stability of the solutions of Equation (16) toward perturbations of R_A is easily discussed if the function $R_A(\psi_A)$ remains valid in the transient system. This condition holds if the effective diffusivities $k/\rho\hat{C}_p$, $\mathcal{D}_1$, $\mathcal{D}_2$, ... $\mathcal{D}_n$ in the particle are equal for all the profiles that affect R_A in Equation (3). Under this condition, the stable solutions are those for which the reactant consumption line crosses the diffusion line from below with increasing ψ_A, as at points 1, 2, 3, 7, 8, 9 and 10 in Figure 2. States where the lines cross the opposite way (Point 5), or meet without crossing (Points 4 and 6), are unstable. These rules are consistent with detailed stability analyses of first-order reactions (*1, 7, 14*).

The effectiveness factor for each steady state can be calculated by quadrature as follows:

$$\eta = \frac{w_1 R_{A1} + w_2 R_{A0}}{R_{A0}} \qquad (17)$$

The coefficients w_1 and w_2 are given in Table 1. This formula, adapted from (*13*), is exact for R_A functions of degree zero through four in each coordinate. Clearly η exceeds unity when R_{A1} exceeds R_{A0}; this is true for solutions 2 through 9 in Figure 2.

DISCUSSION

The relative accuracy of Equations (15) and (17) varies with the particle size. For small particles Equation (17) is accurate, whereas Equation (15) gives values that are too high. For large particles the situation is reversed. Generally speaking, Equation (17) is preferable up to the point where it intersects Equation (15). This is illustrated in Examples 1 and 2.

The collocation method can be extended to larger particle sizes (*13*) by using more terms in the trial function. This approach is better suited to computer use than to graphical treatment; hence we do not use it here.

Table 1 can be applied to other catalyst shapes by using the approximation of Wheeler (*17*) and Aris (*2*) that particles with equal V_p/S_p have nearly equal effectiveness factors. The long cylinder, with D replaced by $4V_p/S_p$, is a convenient model shape for such calculations. The ellipsoid, however, is a more accurate model since it has three length dimensions; thus one can match not only V_p/S_p but also the ratios of three overall particle dimensions.

Heat and mass transfer resistances outside the particle are readily added to this analysis. One can calculate the surface conditions (c_{10}, ... T_0) for several assumed values of the mean reaction rate $\overline{R}_A$, using correlations of transfer coefficients (*18*), and then solve the effectiveness-factor problem at each condition (c_{10}, ... T_0) by the methods given above. The correct solutions may be found graphi-

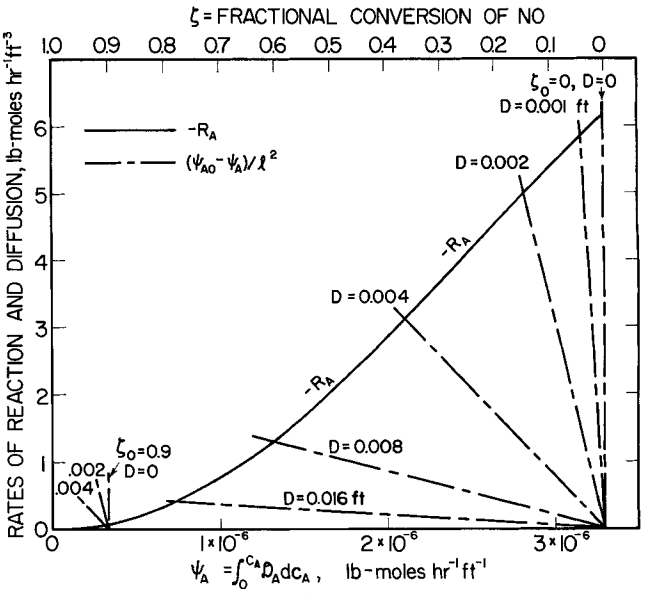

Fig. 3. Graphical solutions of Equation (16) for the Chu-Hougen problem at external conversions of 0.0 and 0.9.

Locus of collocation positions	Coefficient in Equation (16)	Integration weights in Equation (17) w_1	w_2
$\left(\frac{2z}{L}\right)^2 = \frac{1}{5}$	$\frac{1}{l^2} = \frac{10}{L^2}$	$\frac{5}{6}$	$\frac{1}{6}$
$\left(\frac{2r}{D}\right)^2 = \frac{1}{3}$	$\frac{1}{l^2} = \frac{24}{D^2}$	$\frac{3}{4}$	$\frac{1}{4}$
$\left(\frac{2r}{D}\right)^2 = \frac{3}{7}$	$\frac{1}{l^2} = \frac{42}{D^2}$	$\frac{7}{10}$	$\frac{3}{10}$
$\left(\frac{2x}{L_x}\right)^2 + \left(\frac{2y}{L_y}\right)^2 + \left(\frac{2z}{L_z}\right)^2 = \frac{3}{7}$	$\frac{1}{l^2} = \frac{14}{L_x^2} + \frac{14}{L_y^2} + \frac{14}{L_z^2}$	$\frac{7}{10}$	$\frac{3}{10}$

cally by equating ηR_{A0} (calculated) and $\overline{R}_A$ (assumed).

A different collocation method, also based on a parabolic approximating profile, has been given recently by Matsuura and Kato (9). Their method is less accurate than ours in two respects: Their collocation point is located at the particle surface, and their estimate of the reaction rate is obtained by differentiation of the approximate concentration profile rather than integration of R_A. Their method correctly allows for external mass transfer resistance, but fails to show the influence of the internal diffusivity $\mathcal{D}_A$. Thus, their Equation (13) yields an effectiveness factor of unity for all particle sizes.

Example 1. Oxidation of Nitric Oxide

Chu and Hougen (4) have predicted effectiveness factors for the reaction $NO + \frac{1}{2}O_2 \rightarrow NO_2$, catalyzed by spherical particles of activated carbon. They used the rate equation of Kircher and Hougen (6),

$$-R_{NO} = \frac{\rho_p P_{NO}^2 P_{O_2}}{(a + bp_{NO}^2 + cp_{NO_2} + wp_{H_2O})} \quad (18)$$

and considered an isothermal, isobaric, plug-flow reactor at $p = 1.11$ atm. and 329.2°K., with a feed containing 1.50 mole % nitric oxide, 20.24% oxygen, 0.00% nitrogen dioxide, and 0.02% water. The compositions inside and outside the particles were assumed to be identical functions of the local nitric oxide concentration c_A; this assumption is equivalent to setting $\mathcal{D}_i = \mathcal{D}_A$ in Equation (7) for all species. The local reaction rate was thus reduced to a function of the nitric oxide conversion, ζ:

$$-R_A = \frac{(44.4)(1.2176)(26.99 - 54.98\zeta + 28.99\zeta^2 - \zeta^3)}{(133.32 - \zeta)(177.42 - 1.3737\zeta + \zeta^2)} \frac{\text{lb.-moles}}{\text{(hr.)(cu.ft.)}} \quad (19)$$

The effective diffusivity of nitric oxide was assumed constant at 0.0855 sq.ft./hr.; this gives

$$\psi_A = \mathcal{D}_A(c_A - c_{A\,\text{ref.}}) = \frac{0.0581}{133.32 - \zeta_{\text{ref.}}} - \frac{0.0581}{133.32 - \zeta} \frac{\text{lb.-moles}}{\text{(hr.)(ft.)}} \quad (20)$$

as may be verified by combining Equation (35) of Chu and Hougen with our Equation (11).

Figure 3 shows the calculated variation of $-R_A$ with ψ_A, based on the datum $c_{A,\text{ref.}} = 0$. Under the assumptions given for Equation (19), this single curve holds within each particle in the bed. Thus the effectiveness factor can be obtained for any desired location in the reactor, by solving Equation (12) with the local value of ψ_{A0}. Construction lines are shown for the collocation solution at external conversions $\zeta_0 = 0.0$ and 0.9.

Figure 4 shows the calculated effectiveness factors. They increase strongly with conversion; this behavior is typical for isothermal reactions of order greater than unity. The exact values are closely approximated by Equation (17) for $\eta > 0.6$, and by Equation (15) for small values of η. The intervening region can be described within 20% by using the smaller of the two asymptotes, or more accurately by connecting the asymptotes with a smooth curve.

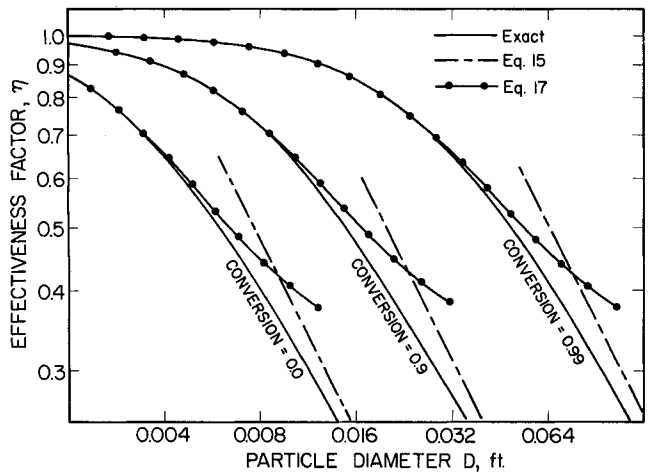

Fig. 4. Calculated effectiveness factors for the Chu-Hougen problem at various external conversions.

Example 2: Multiple Steady States

The problem of nonisothermal first-order reaction in spherical particles, studied by Weisz and Hicks (15), gives a severe test of these graphical procedures. The reaction rate function is

$$\frac{R_A}{R_{A0}} = Y \exp\left\{\frac{\gamma\beta(1-Y)}{1+\beta(1-Y)}\right\} \quad (21)$$

with

$$Y = \frac{c_A}{c_{A0}} \quad (22)$$

$$\gamma = \frac{E}{RT_0} \quad (23)$$

and

$$\beta = \frac{c_{A0}\mathcal{D}_A}{kT_0}\sum_{i=1}^{n}\nu_i\overline{H}_i = \frac{T_{max} - T_0}{T_0} \qquad (24)$$

and is obtained by combining Equation (10) with the Arrhenius rate expression. The effective diffusivity $\mathcal{D}_A$, effective conductivity k, and heat of reaction $\sum \nu_i\overline{H}_i$ are considered constant.

Insertion of Equation (21) into Equation (16), and use of Equation (11), gives the collocation equation

$$\left|\frac{\mathcal{D}_A c_{A0}}{l^2 R_{A0}}\right|(1 - Y_1) = Y_1 \exp\left\{\frac{\gamma\beta(1 - Y_1)}{1 + \beta(1 - Y_1)}\right\} \qquad (25)$$

For spheres this becomes

$$\frac{10.5}{\phi^2}(1 - Y_1) = Y_1 \exp\left\{\frac{\gamma\beta(1 - Y_1)}{1 + \beta(1 - Y_1)}\right\} \qquad (26)$$

in which ϕ is the Thiele modulus:

$$\phi = \frac{D}{2}\sqrt{\frac{|R_{A0}|}{\mathcal{D}_A c_{A0}}} \qquad (27)$$

Equation (26) can be solved in the same manner as Equation (16), by plotting both terms vs. Y. The construction is shown in Figures 5, 6, and 7 for various values of the parameters β and ϕ.

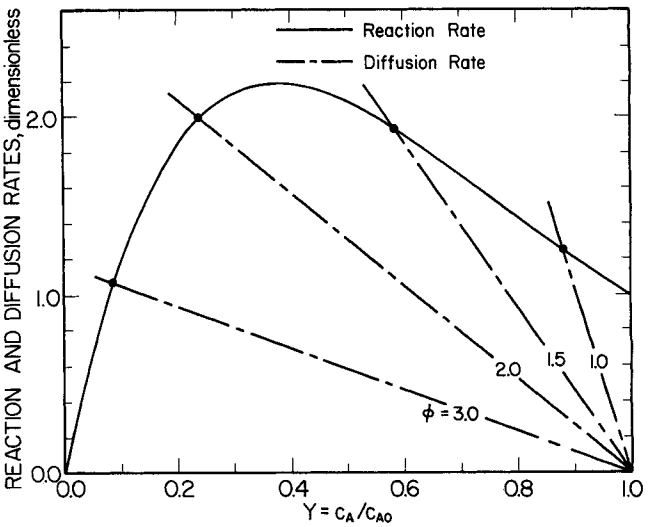

Fig. 6. Solutions of Equation (26) with $\gamma = 30$ and $\beta = 0.1$ (exothermic).

The behavior of the solutions depends on the heat effect, and on the sign of the activation energy, E. Consider the usual situation, where E is positive. Then for endothermic reactions (negative β) as in Figure 5, there is just one solution of Equation (26) for each set of external conditions, and R_{A1} is always less than R_{A0}, giving an effectiveness factor less than unity. For moderately exothermic conditions (small positive β) as in Figure 6, unique solutions are still obtained, but R_{A1} may exceed R_{A0}, giving effectiveness factors above unity. For highly exothermic reactions, as in Figure 7, the solution becomes triple valued over a range of ϕ. The middle solution of the three is unstable and the outer two are stable, by the criteria previously given.

The effectiveness factors corresponding to Figure 7 are shown in Figure 8. The collocation method [Equations (17) and (26)] predicts η accurately to the left of the multiple solution region, and closely predicts the extent of the region. The large particle asymptote becomes accurate to the right of the multiple solution region. Operation on the left side would normally be preferred, since this region gives more reasonable temperatures inside the catalyst particles.

The limits of the multiple solution region, ϕ_{max} and

Table 2. Calculated Limits of the Multiple-Solution Region in the Weisz-Hicks Problem

		$\beta = 0.2$		$\beta = 0.3$		$\beta = 0.4$		$\beta = 0.6$		$\beta = 0.8$	
		ϕ_{min}	ϕ_{max}	ϕ_{min}	ϕ_{max}	ϕ_{min}	ϕ_{max}	ϕ_{min}	ϕ_{max}	ϕ_{min}	ϕ_{max}
$\gamma = 20$	exact*	none	none	**0.859**	**0.873**	0.58	0.73	0.30	0.57	**0.155**	**0.510**
	Equation (26)	none	none	0.863	0.932	0.555	0.776	0.252	0.613	0.131	0.530
	Equation (21) of ref. 8	not less than 1.448	—	not less than 0.757	—	not less than 0.434	—	not less than 0.175	—	not less than 0.086	—
	exact*	0.79	0.87	0.41	0.68	0.22	0.58	**0.074**	**0.465**	—	—
$\gamma = 30$	Equation (26)	0.784	0.916	0.355	0.714	0.170	0.606	0.049	0.487	0.018	0.416
	Equation (21) of ref. 8	not less than 0.651	—	not less than 0.247	—	not less than 0.108	—	not less than 0.028	—	not less than 0.0098	—

* Values in bold type were obtained by the method of reference 13, with 12 collocation points. The other exact values are from the graphs of Weisz and Hicks (15).

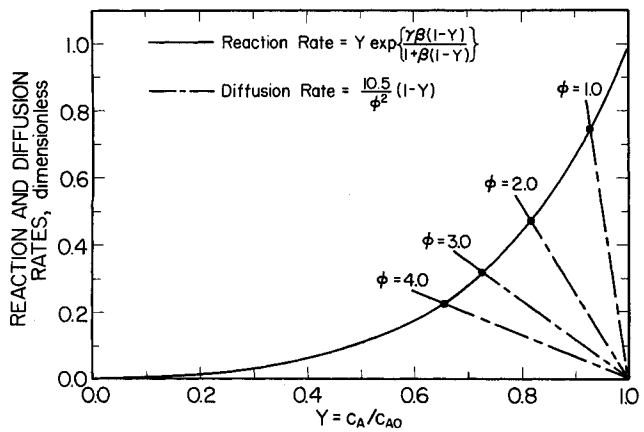

Fig. 5. Solutions of Equation (26) with $\gamma = 30$ and $\beta = -0.1$ (endothermic).

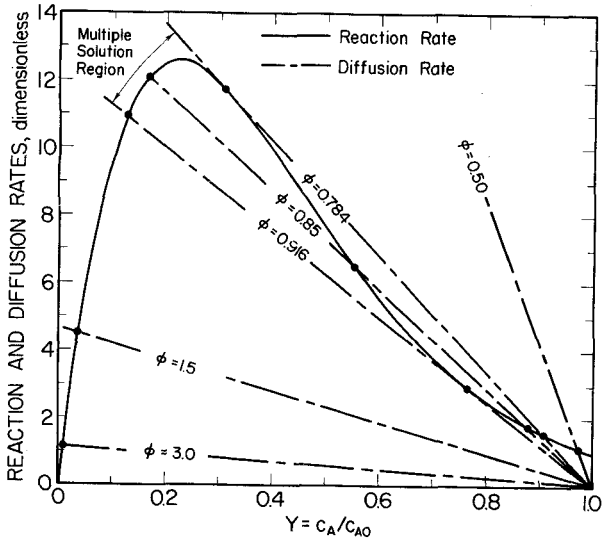

Fig. 7. Solutions of Equation (26) with $\gamma = 30$ and $\beta = 0.2$ (exothermic).

ϕ_{min}, are shown for other conditions in Figure 9 and Table 2. The predictions by the collocation method are good, ranging from 1.03 to 1.08 times the exact values for ϕ_{max}, and 0.66 to 1.003 times the exact values for ϕ_{min}. The lower bounds on ϕ_{min} given by the Luss-Amundson theorem (8) are more conservative, as shown in Table 2.

Example 3: Criteria for Kinetically-Controlled Reaction

Chemical kinetic studies are best done with small catalyst particles, to avoid thermal and diffusional complications. Equations (16) and (17) can be used to determine how small the particles must be to stay within given tolerances on η. The criteria obtained are simple, and more general than those currently available (*16, 15, 3*).

If η is to be kept in the range 1.0 ± 0.05, then Equation (17) indicates that R_{A1} must be kept within $(5/w_1)$ percent of R_{A0}:

$$\left| \frac{R_{A1} - R_{A0}}{R_{A0}} \right| \leq \frac{0.05}{w_1} \qquad (28)$$

If a plot of $-R_A$ vs. ψ_A is available (drawn from preliminary experiments and estimates), then we can find the critical values R_{A1} and ψ_{A1} that just satisfy criterion (28). The maximum permissible value of l then follows from Equation (16) and the corresponding particle dimensions can be found from Table 1.

The calculation can be approximated analytically by

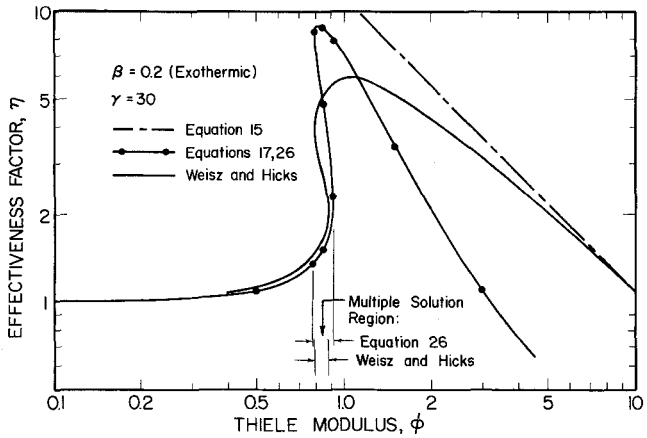

Fig. 8. Effectiveness factors for $\gamma = 30$ and $\beta = 0.2$. The plotted points correspond to the solutions in Figure 7.

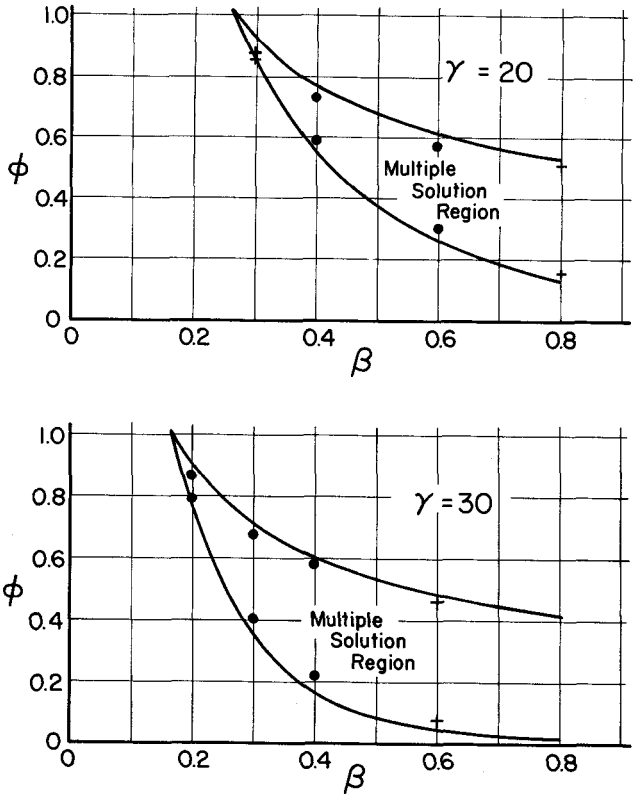

Fig. 9. Limits of multiple-solution region for the Weisz-Hicks problem at $\gamma = 20$ and $\gamma = 30$. Curves are from Equation (26); dots, from plots of Weisz and Hicks; crosses are exact values computed by 12 point collocation.

expanding R_A in a truncated Taylor series:

$$R_A = R_{A0} + (\psi_A - \psi_{A0}) \left(\frac{dR_A}{d\psi_A} \right)_{c_0,\, T_0} \qquad (29)$$

Here the subscripts c_0, T_0 denote a fixed state at the outer surface of the particle. Equations (28) and (16) then give

$$l^2 \left(\frac{w_1}{0.05} \pm 1 \right) \left| \frac{dR_A}{d\psi_A} \right|_{c_0,\, T_0}$$

$$\equiv l^2 \left(\frac{w_1}{0.05} \pm 1 \right) \left| \frac{1}{\mathcal{D}_{A0}} \frac{dR_A}{dc_A} \right|_{c_0,\, T_0} \leq 1 \qquad (30)$$

as the restriction on l for a $\pm 5\%$ tolerance on η. The ± 1 term is unimportant, but if retained it should be given the same sign as $\mathcal{D}_A dR_A/dc_A$. This result is correct provided that Equation (29) is accurate throughout the particle, that is, from ψ_{A0} to about $\psi_{A0} + 2l^2 R_{A0}$ for the geometries in Table 1.

For exploratory work, Criterion (30) is inconvenient because the derivative dR_A/dc_A is unknown. The estimation of this quantity can be simplified by introducing a relative rate function $g_A(\psi_A) = R_A/R_{A0}$ and a measured reaction rate value, $\overline{R}_A = \eta R_{A0}$ for particles of a given characteristic length l. The criterion then becomes:

$$l^2 \left(\frac{w_1}{0.05} \pm 1 \right) \left| \frac{\overline{R}_A}{(1 \pm 0.05)\, \mathcal{D}_{A0}} \right| \left| \frac{dg_A}{dc_A} \right|_{c_0,\, T_0} \leq 1 \qquad (31)$$

Here (1 ± 0.05) represents the effectiveness factor at the limit of Criterion (28), and the sign is the same as for the ± 1 term. Note that both l^2 and $\overline{R}_A$ in criterion (31)

depend on the particle size; their product, however, decreases with l so that the criterion is satisfied for small particle sizes.

For illustration, consider an isothermal irreversible reaction of order $n > 0$, catalyzed by porous spherical particles. In this system $R_A = R_{A0}(c_A/c_{A0})^n$, $w_1 = 7/10$, and $l = D/\sqrt{42}$. Inequalities (30) and (31) give

$$D^2 \left| \frac{n R_{A0}}{\mathcal{D}_{A0} c_{A0}} \right| \leq \frac{42}{13} \tag{32}$$

and

$$D^2 \left| \frac{n \bar{R}_A}{\mathcal{D}_{A0} c_{A0}} \right| \leq (0.95) \frac{42}{13} \tag{33}$$

as equivalent criteria of the kinetically-controlled region. When $n = 1$, these criteria give results similar to Equations (26) and (27) of Weisz and Prater (*16*).

Criteria (30) and (31) are simple and widely applicable. They provide more accurate bounds than any previously available criteria. The bounds on η can be changed to $1 \pm \epsilon$, if desired, by changing 0.05 to ϵ in Equations (28), (30), and (31). The equations thus modified will give accurate results as long as the tolerance, ϵ, is small relative to w_1.

CONCLUSION

Equations (15), (16), and (17), and Table 1 are the key results in this development. These equations predict η in terms of the reaction rate law, the transport properties, and the particle size and shape. The predictions in the moderate particle-size range are markedly improved over existing approximation methods.

This development has been purposely limited to simple methods for graphical use. This entails some sacrifice of accuracy, but a gain in understanding. The graphical methods should provide useful guidance in reactor analysis, design and operation, particularly where multiple solutions are involved.

ACKNOWLEDGMENT

This work was supported by the National Science Foundation, Grant GK-678, and by a North Atlantic Treaty Organization Science Fellowship for J. V. Villadsen.

NOTATION

A = species chosen as basis in Equation (3)
$a_0^{(1)}$ = coefficient in Table 1; depends on reaction rate function, particle size and particle shape
$\hat{C}_p$ = heat capacity, smoothed over pores and solid
c_i = concentration of species i (moles L^{-3})
D = diameter of cylinder or sphere
$\mathcal{D}_i$ = effective diffusivity of species i in particle
E = activation energy
$g(\psi_A)$ = $R_A(\psi_A)/R_{A0}$, relative reaction rate function
$\overline{H}_i$ = partial molar enthalpy of species i
k = effective thermal conductivity of particle
k_n = nth order pseudo-homogeneous reaction rate constant
L = thickness of slab
L_x, L_y, L_z = axes of ellipsoid
l = characteristic length defined in Table 1
$\mathbf{N}_i$ = local flux vector of species i, relative to particle, smoothed over pores and solid (moles $L^{-2}t^{-1}$)
$|N_{A0}|$ = magnitude of $\mathbf{N}_A$ at outer particle surface
n = reaction order
$\mathbf{q}^{(c)}$, $\mathbf{q}^{(x)}$ = contributions of temperature gradient and concentration gradients to local energy flux, relative to particle, smoothed over pores and solid ($E\,L^{-2}\,t^{-1}$)
R = gas constant
R_i = rate of production of species i, smoothed over pores and solid (moles $L^{-3}\,t^{-1}$)
R_{A0} = rate of production of A in outermost layer of catalyst particle (moles $L^{-3}\,t^{-1}$)
$\overline{R_A}$ = mean rate of production of A over the particle volume (moles $L^{-3}\,t^{-1}$)
r = radial coordinate in cylinder or sphere
S_p = external surface area of particle
T = temperature
T_{max} = internal particle temperature corresponding to $c_A = 0$ in Example 2
V_p = volume of particle
w_1, w_2 = coefficients in Equation (17)
X = dimensionless coordinate, equal to $2z/L$ for slabs, $2r/D$ for cylinders and spheres, and $[(2x/L_x)^2 + (2y/L_y)^2 + (2z/L_z)^2]^{1/2}$ for ellipsoids
x, y, z = rectangular coordinates measured from center of particle

Greek Letters

β = $(T_{max} - T_0)/T_0$; see Equation (24)
γ = E/RT_0
ζ = conversion of nitric oxide
η = effectiveness factor
ν_i = stoichiometric coefficient, defined as moles of i produced per mole of A produced; see Equation (3)
ρ_p = local particle density, including pores and solid
ϕ = Thiele modulus; see Equation (27)
ψ_A = diffusion potential; see Equation (11)
$\psi_A^{(1)}$ = collocation approximation to ψ_A with one adjustable coefficient

Subscripts

A = species chosen as basis
e = equilibrium
i = any one of the species
ref. = reference state in Equation (11)
0 = state at the particle exterior [exception: $a_0^{(1)}$ is the coefficient for $i = 0$ in the notation of (*13*)]
1 = state at the collocation positions

LITERATURE CITED

1. Amundson, N. R., and L. R. Raymond, *AIChE J.*, **11**, 339 (1965).
2. Aris, Rutherford, *Chem. Eng. Sci.*, **6**, 265 (1957).
3. Bischoff, K. B., *ibid.*, **22**, 525 (1967).
4. Chu, Chieh, and O. A. Hougen, *ibid.*, **17**, 167 (1962).
5. Gavalas, G. R., *ibid.*, **21**, 477 (1966).
6. Kircher, Omer, and O. A. Hougen, *AIChE J.*, **3**, 331 (1957).
7. Kuo, J. C. W., and N. R. Amundson, *Chem. Eng. Sci.*, **22**, 49, 443, 1185 (1967).
8. Luss, Dan, and N. R. Amundson, *ibid.*, **22**, 253 (1967).
9. Matsuura, T., and M. Kato, *ibid.*, **22**, 171 (1967).
10. Peterson, E. E., *ibid.*, **17**, 987 (1962).
11. Peterson, E. E., "Chemical Reaction Analysis," Sect. 4.4, Prentice-Hall, Englewood Cliffs, N.J. (1965).
12. Bird, R. B., W. E. Stewart, and E. N. Lightfoot, "Notes on Transport Phenomena," pp. 335-341, John Wiley, New York (1958).
13. Villadsen, J. V., and W. E. Stewart, *Chem. Eng. Sci.*, **22**, 1483 (1967).
14. Wei, James, *ibid.*, **20**, 729 (1965).
15. Weisz, P. B., and J. S. Hicks, *ibid.*, **17**, 265 (1962).
16. ———, and C. D. Prater, *Advan. Catalysis*, **6**, 167 (1954).
17. Wheeler, Ahlborn, *ibid.*, **3**, 258, 294 (1951).
18. Yoshida, Fumitake, D. Ramaswami, and O. A. Hougen, *AIChE J.*, **8**, 5 (1962). See also Bird, R. B., W. E. Stewart, and E. N. Lightfoot, "Transport Phenomena," Chapt. 21, John Wiley, New York (1960).

Manuscript received February 5, 1968; revision received April 11, 1968; paper accepted April 15, 1968. Paper presented at AIChE Los Angeles meeting.